Binding Mechanism of the Peptidoglycan Hydrolase Acm2: Low Affinity, Broad Specificity

Audrey Beaussart, Thomas Rolain, Marie-Clémence Duchêne, Sofiane El-Kirat-Chatel, Guillaume Andre, Pascal Hols,* and Yves F. Dufrêne*
Université catholique de Louvain, Institute of Life Sciences, Croix du Sud, Louvain-la-Neuve, Belgium

ABSTRACT Peptidoglycan hydrolases are bacterial secreted enzymes that cleave covalent bonds in the cell-wall peptidoglycan, thereby fulfilling major physiological functions during cell growth and division. Although the molecular structure and functional roles of these enzymes have been widely studied, the molecular details underlying their interaction with peptidoglycans remain largely unknown, mainly owing to the paucity of appropriate probing techniques. Here, we use atomic force microscopy to explore the binding mechanism of the major autolysin Acm2 from the probiotic bacterium *Lactobacillus plantarum*. Atomic force microscopy imaging shows that incubation of bacterial cells with Acm2 leads to major alterations of the cell-surface nanostructure, leading eventually to cell lysis. Single-molecule force spectroscopy demonstrates that the enzyme binds with low affinity to structurally different peptidoglycans and to chitin, and that glucosamine in the glycan chains is the minimal binding motif. We also find that Acm2 recognizes mucin, the main extracellular component of the intestinal mucosal layer, thereby suggesting that this enzyme may also function as a cell adhesion molecule. The binding mechanism (low affinity and broad specificity) of Acm2 may represent a generic mechanism among cell-wall hydrolases for guiding cell division and cell adhesion.

INTRODUCTION

Peptidoglycan is a bacterial polymer made up of glycan strands cross-linked by short peptides, which provides remarkable mechanical strength to the bacterial cell wall (1,2). Glycan chains are composed of repeating units of the disaccharide *N*-acetylglucosamine-*N*-acetylmuramic acid (GlcNAc-MurNAc), whereas interpeptide bridges are classically made of alternating L- and D-amino acids attached to *N*-acetylmuramic acids, the composition of which varies from species to species. Peptidoglycan forms a highly dynamic network that allows the cells to grow and divide while maintaining their shape and integrity. Peptidoglycan remodeling during cell division and growth involves two machineries, one for elongation, the other for division. The division machinery relies on various proteins, among which peptidoglycan hydrolases, i.e., bacterial secreted enzymes that cleave covalent bonds in the cell wall peptidoglycan at specific times and sites during cell growth (3,4). These enzymes are known to play a number of crucial physiological functions, including the regulation of cell-wall growth, the turnover of peptidoglycan during growth, the separation of daughter cells during cell division, and autolysis (4).

Four main classes of peptidoglycan hydrolases have been distinguished, including the *N*-acetylglucosaminidases, which hydrolyze the GlcNAc-MurNAc bond of the glycan chains. A prominent example of *N*-acetylglucosaminidase is Acm2, the major autolysin of the probiotic bacterium *Lactobacillus plantarum* (5). Acm2 is a modular protein composed of an N-terminal alanine-, serine-, and threonine-rich region (AST domain), a central catalytic domain, and a C-terminal region made of five SH3b repeats previously shown to bind peptidoglycan (6,7). However, the binding mechanism (affinity, specificity) of the SH3b domain remains poorly understood. In particular, the binding motif recognized by SH3b is unclear, since several studies have shown a predominant role of either interpeptidic bridges or glycan strands (6–8). Also, whether the SH3b domain is capable of binding targets other than peptidoglycans is not known.

During the past years, atomic force microscopy (AFM) has provided new insights into the molecular organization and interactions of bacterial cell-wall constituents (9–11), including peptidoglycans (12–14). In particular, single-molecule force measurements enable researchers to manipulate single-cell proteins, thereby offering a means to measure their molecular elasticity, unfolding/refolding pathways, and specific binding forces (15,16). Whether AFM can unravel the binding strength, affinity, and specificity of Acm2 is the question we address here. AFM images of single *L. plantarum* cells show that Acm2 causes major changes of the cell-surface structure, leading eventually to cell lysis. Single-molecule force measurements reveal that the enzyme binds with low affinity to *L. plantarum* cells, peptidoglycan purified from various species, chitin, and mucin. Blocking experiments demonstrate that glucosamine is the minimal binding motif. Collectively, our results emphasize that Acm2 binds with low affinity and broad specificity, a feature that could be common to peptidoglycan hydrolases of many probiotic and pathogenic bacteria.

Submitted May 24, 2013, and accepted for publication June 25, 2013.

*Correspondence: yves.dufrene@uclouvain.be or pascal.hols@uclouvain.be

Editor: Andreas Engel.

0006-3495/13/08/0620/10 $2.00

http://dx.doi.org/10.1016/j.bpj.2013.06.035

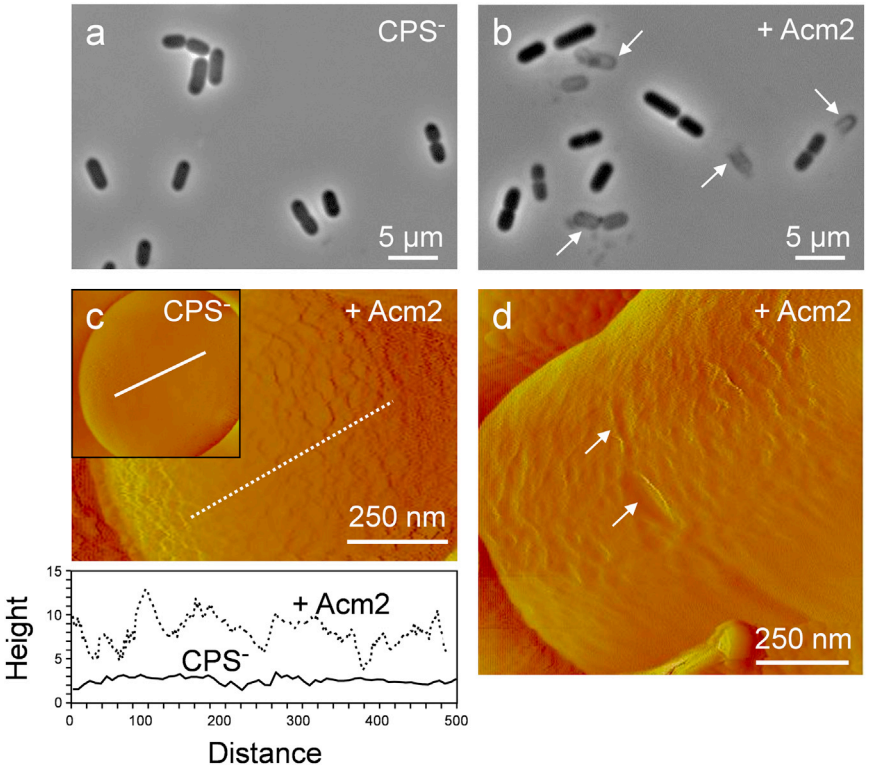

FIGURE 1 Phenotype analysis and nanostructural imaging of the lytic activity of Acm2. (*a* and *b*) Light (bright-field) microscopy images of *L. plantarum* cells (CPS null mutant (CPS^-)) before (*a*) and after (*b*) incubation with 40 $\mu g\ mL^{-1}$ Acm2 in phosphate buffer at pH 5.8 for 2 h at 30°C without agitation. White arrows in *b* show cell debris resulting from enzyme activity. (*c* and *d*). AFM deflection images recorded with a silicon nitride tip, in contact mode, at a minimum applied force (<100 pN) for the pole (*c*) and side walls (*d*) of CPS^- cells after incubation with 40 $\mu g\ mL^{-1}$ Acm2 in phosphate buffer for 2 h at 30°C. The inset in *c* shows an image of a nontreated cell pole, as well as vertical cross sections taken in height images of the poles of native (*solid line*) and treated (*dashed line*) cells. White arrows in *d* show nanoscale perforations in the septum region. Similar data were obtained with different cells from independent cultures.

MATERIALS AND METHODS

Bacterial strains and growth conditions

L. plantarum NZ7100 cells, as well as a capsular polysaccharide (CPS) null mutant constructed by deleting the four gene clusters potentially involved in CPS synthesis (17) were grown in Mann-Rogosa-Shape broth (Difco, Franklin Lakes, NJ) at 30°C without agitation. Overnight cultures were harvested by centrifugation and washed three times in phosphate buffer at pH 5.8. *L. lactis* recombinant strains were grown in M17 broth (BD Biosciences, San Jose, CA) containing 0.5% glucose (M17-glucose) in the presence of chloramphenicol (10 $\mu g\ mL^{-1}$) at 30°C. *L. lactis* strains NZ3900 (pGITR0014) and NZ3900 (pGITR0016) were used for the purification of Acm2 and its deleted variant Acm2ΔSH3, respectively (18).

Acm2 production and purification

Acm2-tagged proteins were overproduced in *L. lactis* using the NICE system (18). Expression was induced with Nisin A (Sigma-Aldrich, St. Louis, MO) at a concentration of 2 ng mL^{-1}. Bacteria were grown to mid-exponential phase ($OD_{600} = 0.8$) and harvested by centrifugation at 5000 × *g* for 10 min at 4°C. The pellet was washed once with 50 mM potassium phosphate buffer, pH 8.0, and resuspended at an OD_{600} of 80 in 50 mM potassium phosphate buffer, pH 8.0. Cells were lysed with glass beads using a Precellys cell disrupter (Bertin Technologies, Aix en Provence, France) at 5000 rpm for 5 × 30 s and then centrifugated at 20,000 × *g* for 20 min at 4°C. To obtain homogeneous preparations of the proteins, these were subjected to two consecutive purifications. To this end, proteins were modified N-terminally by a His_6-tag and C-terminally by a Strep-tag. They were then purified successively by affinity chromatography on Ni^{2+} with the Pro-Bond Purification System (Inivtrogen, Carlsbad, CA) and with the Strep-Tactin-Superflow 1 mL columns (IBA, Goettingen, Germany) according to the instructions of the manufacturers, followed by an overnight dialysis step against phosphate buffer at pH 5.8. Protein concentration was measured using the Bio-Rad (Hercules, CA) Protein Assay. The purity and integrity of the tagged proteins were checked by sodium dodecyl sulfate polyacrylamide gel electrophoresis before storing at 4°C.

Preparation of peptidoglycan, chitin, and mucin surfaces

Peptidoglycans from *Bacillus subtilis*, *Staphylococcus aureus*, and *Micrococcus luteus*, chitin (from shrimp shells), and mucin (from porcine stomach, type III) (all from Sigma) were covalently immobilized onto gold substrates. Silicon wafers coated by thermal evaporation with a thin layer of Cr (~5 nm) followed by a thin layer of gold (~30 nm) were cleaned for 15 min by ultraviolet-ozone treatment, rinsed in ethanol, and dried with N_2. The clean substrates were immersed overnight in a 1 mM thiol solution of 90% mercapto-1-undecanol and 10% mercaptohexadecanoic acid (both from Sigma), rinsed in ethanol, briefly sonicated in ethanol solution, and dried with N_2. Substrates were then immersed for 30 min in a solution of 10 $g\ L^{-1}$ N-hydroxysuccinimide (NHS) and 25 $g\ L^{-1}$ *N*-(3-dimethylaminopropyl)-*N′*-ethylcarbodiimide hydrochloride (EDC) (Sigma), rinsed with MilliQ water (ultrapure water from Millipore (Elga LabWater); resistivity of 18.2 MΩ·cm at 25°C), incubated for 1 h with a 100 $\mu g\ mL^{-1}$ solution of peptidoglycan or chitin, or 10 mg mL^{-1} solution of mucin, rinsed with buffer, and immediately used.

AFM measurements

AFM images and force-distance curves were obtained in phosphate buffer at pH 5.8 at room temperature unless otherwise stated, using a Nanoscope V Multimode AFM (Bruker, Santa Barbara, CA). When working with live bacteria, cells were immobilized by mechanical trapping into porous polycarbonate membranes (Millipore) with a pore size similar to the bacterial cell size (19). Before use, membranes were maintained overnight at 110°C and then cooled at room temperature. After filtering a cell culture,

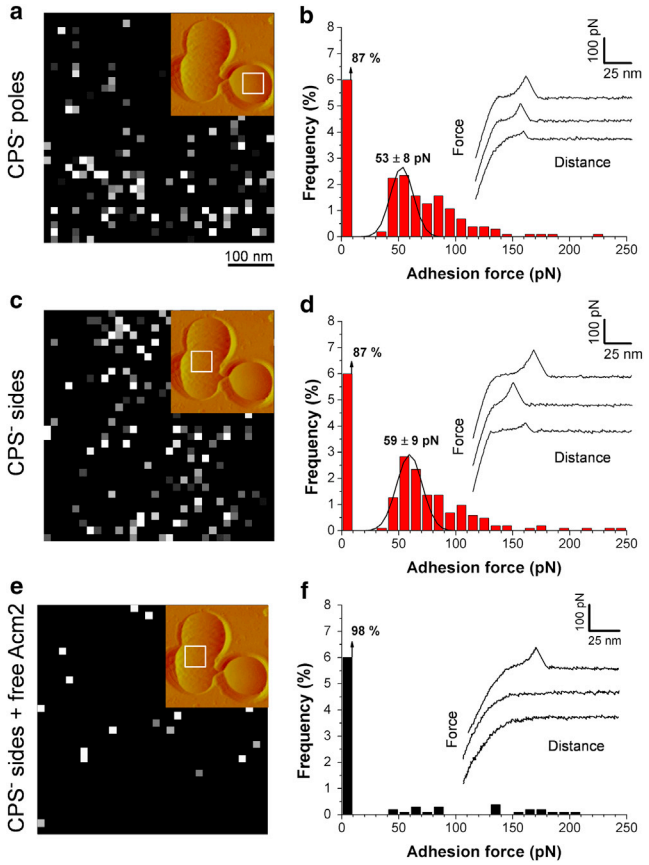

FIGURE 2 Detecting and localizing single Acm2-peptidoglycan interactions on whole cells. Adhesion-force maps (500 nm × 500 nm; gray scale, 100 pN) (*a*, *c*, and *e*), and adhesion-force histograms ($n = 1024$) (*b*, *d*, and *f*) with representative force curves, recorded in buffer with an Acm2 tip on the pole of a native CPS^- mutant cell (*a* and *b*), and on the side wall of a CPS^- mutant cell before (*c* and *d*) and after (*e* and *f*) incubation with 100 $\mu g\ mL^{-1}$ Acm2 for 1 h. Similar data were obtained in three independent experiments using different tip preparations and cell cultures.

the filter was gently rinsed with the buffer, carefully cut (1 cm × 1 cm), and attached to a steel sample puck (Bruker) using a small piece of double face adhesive tape. The mounted sample was transferred into the AFM liquid cell with care taken to avoid dewetting. For single-molecule force measurements, samples (live bacteria, model substrates) were first imaged using a bare silicon nitride tip (MSCT, Bruker) under minimal applied force, after which the tip was changed with an Acm2-functionalized tip (see below). Adhesion maps on live cells were obtained by recording 32 × 32 force-distance curves on areas of a given size, calculating the adhesion force for each force curve, and displaying the value as a gray pixel. For measurements on model surfaces, the presence and homogeneity of biomolecular layers was checked by imaging the substrate with a bare tip. The tip was then exchanged with an Acm2-functionalized tip to perform force measurements at different locations on the substrates. Inhibition experiments were performed by injecting 1 mM solutions of the monosaccharides D-glucose, D-glucosamine, *N*-acetyl-D-glucosamine, muramic acid, and *N*-acetyl muramic acid (all from Sigma). Unless stated otherwise, all force curves were obtained using a contact time of ~100 ms, a maximum applied force of 250 pN, and approach and retraction speeds of 1000 nm/s. To account for the flexibility of the biomolecules, loading rates ($pN\ s^{-1}$) were estimated by multiplying the tip retraction velocity ($nm\ s^{-1}$) by the slope of the rupture peaks ($pN\ nm^{-1}$). The spring constants of the cantilevers were measured using the thermal noise method (Nanoscope software version 7.30, Bruker). For force data analysis, we constructed adhesion force histograms and plots by extracting the maximum adhesion force for each adhesive curve using the Nanoscope software.

AFM tips were functionalized with Acm2 proteins in a random orientation, using ~6 nm long PEG-benzaldehyde linkers as described by Ebner et al. (20). Cantilevers were washed with chloroform and ethanol, placed in an ultraviolet-ozone cleaner for 30 min, immersed overnight in an ethanolamine solution (3.3 g ethanolamine in 6 mL of dimethylsulfoxide), then washed three times with dimethylsulfoxide and two times with ethanol, and dried with N_2. The ethanolamine-coated cantilevers were immersed for 2 h in a solution prepared by mixing 1 mg Acetal-PEG-NHS dissolved in 0.5 mL chloroform with 10 μL triethylamine, then washed with chloroform and dried with N_2. Cantilevers were further immersed for 10 min in a 1% citric acid solution, washed with MilliQ water, and then covered with a 200 μL droplet of Acm2 solution (0.2 $mg\ mL^{-1}$) to which 2 μL of a 1 M $NaCNBH_3$ solution were added. After 50 min, cantilevers were incubated with 5 μL of a 1 M ethanolamine solution to passivate unreacted aldehyde groups, then washed and stored in phosphate buffer.

RESULTS AND DISCUSSION

Acm2 induces major alterations of the *L. plantarum* surface ultrastructure

Given its role in daughter cell separation and autolysis (5,18,21,22), Acm2 is expected to alter the cell wall ultrastructure. To address this issue, *L. plantarum* cells incubated with free Acm2 were examined using optical microscopy and AFM imaging. As peptidoglycan is covered with a layer of polysaccharides in wild-type (WT) *L. plantarum* (23), we used a mutant in which the four gene clusters potentially involved in CPS synthesis are deleted (Δ*cps1–4* strain) (17). Earlier phenotype analysis and AFM imaging showed that cell growth and cell surface nanostructure of the CPS^- mutant are similar to those of the WT (17). In addition, this mutant strain was recently shown to improve Acm2 binding due to a better access to peptidoglycan (24). Optical microscopy images revealed that incubation of CPS^- mutant cells with a solution of Acm2 (40 $\mu g\ mL^{-1}$, 2 h at 30°C) yielded many ghost cells and cell debris, reflecting the lytic activity of the enzyme (Fig. 1, *a* and *b*). High-resolution AFM imaging demonstrated that Acm2 had a profound impact on the surface nanomorphology of the cells (Fig. 1, *c* and *d*). Fig. 1 *c* shows that Acm2 induced a major increase of the surface roughness of the poles, from ~1.5 nm to ~4.5 nm (root-mean-square roughness on 500 nm × 500 nm measured on height images; for comparison, the roughness of nontreated WT poles was ~0.5 nm). Moreover, nanoscale perforations were seen in the septum region that were never observed on native cells (17). Similar structures were reported for *S. aureus* at the onset of division and attributed to regions of the cell wall having high autolytic activity (25). Also, the increased roughness and pore formation are reminiscent of the effects observed by treating *S. aureus* cells with lysostaphin, an enzyme that hydrolyzes the pentapeptide cross-linkages of peptidoglycans (26). Taken together, our AFM images demonstrate that Acm2

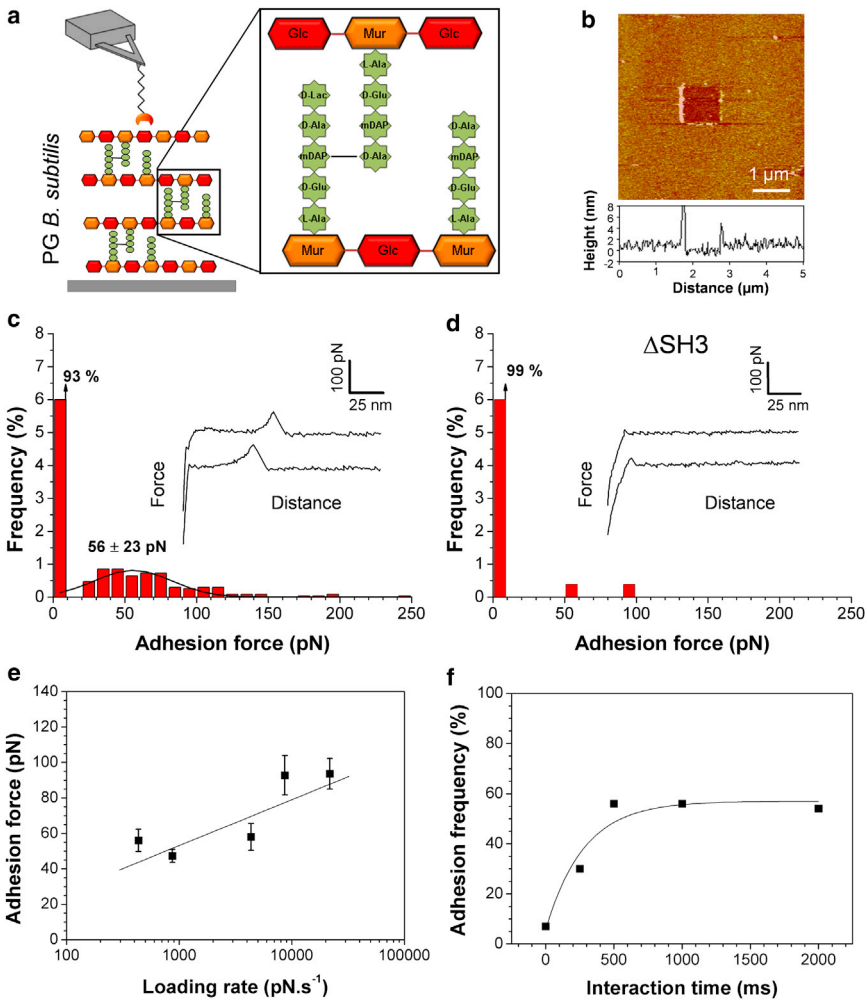

FIGURE 3 Strength and dynamics of the Acm2-peptidoglycan interaction. (*a*) Strategy for measuring the interaction between Acm2 and peptidoglycan. Peptidoglycan purified from *B. subtilis* was chosen, as it is structurally similar to that of *L. plantarum*, with interpeptide bridges composed of L-Ala, D-Glu, mesodiaminopimelic acid (mDAP), D-Ala, and D-lactate as the last moiety (22). Acm2 proteins were attached to AFM tips using a polyethylene glycol linker, whereas peptidoglycan was covalently attached to carboxyl-terminated surfaces via NHS/EDC chemistry. In the schematic of the *B. subtilis* peptidoglycan structure, red and orange represent GlcNAc and MurNAc monosaccharides, respectively, whereas green corresponds to the pentapeptide bridges. (*b*) AFM height image ($z = 10$ nm; a vertical cross section taken in the center of the image is shown beneath the image) recorded with a silicon nitride tip documenting the presence of a smooth, homogeneous layer of peptidoglycan. To determine the layer thickness (~1.3 nm), a small square area was first scanned at large forces (>10 nN), after which a larger image of the same area was recorded at smaller forces. (*c*) Adhesion-force histogram, with representative force curves, recorded in buffer between an Acm2 tip and a peptidoglycan surface. The data shown correspond to 2000 force curves obtained from six independent experiments (different tips and substrates). (*d*) Similar experiment in which the AFM tip was functionalized with the deleted variant Acm2ΔSH3 instead of the full-length Acm2 protein. (*e*) Dependence of the adhesion force on the loading rate applied during retraction (mean ± SE of $n = 200$ force curves for each data point). (*f*) Dependence of the adhesion frequency on the interaction time, measured at a constant retraction speed of 1000 nm/s. To build this plot, only the curves showing single-molecule adhesion events were considered. Similar loading-rate and interaction-time plots were obtained in duplicate experiments using different tips and substrates.

causes substantial alteration of the cell wall, attributed to peptidoglycan digestion and leading eventually to cell lysis.

Acm2 binds to *L. plantarum* cells

Biochemical and microscopy studies have revealed that the SH3b domain of Acm2 binds peptidoglycan (24), but the molecular mechanisms of this interaction are not known. We used single-molecule AFM with tips functionalized with Acm2 to detect, localize and quantify single Acm2-peptidoglycan interactions on *L. plantarum* cells. Fig. 2, *a–d* shows adhesion force maps and histograms, with representative force curves, recorded between the Acm2 tip and the surface of CPS^- mutant cells. A substantial proportion (13%) of force curves showed adhesion events randomly distributed across the surface, with no major difference observed between the cell poles and the side walls (Fig. 2, *b* and *d*). The adhesion-force histograms showed maxima centered at 53 ± 8 pN (mean ± SD; n = 1024 curves; similar force values were obtained using three different tips and cell cultures) and 59 ± 9 pN on the poles and side walls, respectively, which, for several reasons, we believe reflects the rupture of single Acm2-peptidoglycan complexes. First, the specificity of the interaction was confirmed by showing a dramatic reduction of adhesion probability when performing the same experiment in a solution containing 100 μg mL^{-1} of Acm2 (Fig. 2, *e* and *f*). Second, the adhesion values are in the range of those obtained at fairly comparable loading rates for other receptor-ligand complexes (27). Third, binding strengths in the same range were recently measured for the specific interaction between peptidoglycan and the LysM motif present in the *N*-acetylglucosaminidase AcmA from *L. lactis* (13,14). Fourth, we observed very poor binding between Acm2 and the surface of WT cells, confirming that in the WT, peptidoglycan is

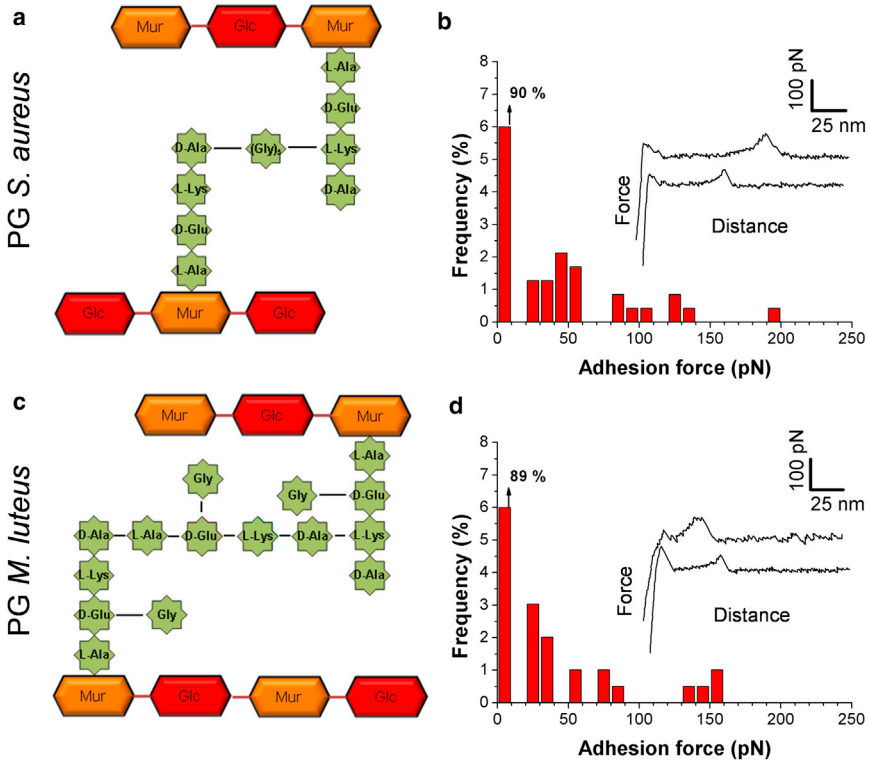

FIGURE 4 Interaction between Acm2 and structurally different peptidoglycans. (*a* and *c*) Structure of the *S. aureus* (*a*) and *M. luteus* (*c*) peptidoglycans, emphasizing differences in interpeptide bridges. (*b* and *d*) Adhesion-force histograms ($n = 200$), with representative force curves, recorded in buffer between Acm2 tips and *S. aureus* (*b*) or *M. luteus* (*d*) peptidoglycans. Similar data were obtained in duplicate experiments using different tips and substrates.

covered with an outer layer of polysaccharides (23). Taken together, these observations suggest that Acm2 specifically binds to surface-exposed peptidoglycan in *L. plantarum* cells. Note that binding forces up to 100–150 pN were sometimes observed, reflecting the simultaneous detection of two or three molecules.

Dynamics of the Acm2-peptidoglycan interaction

To explore the dynamics and specificity of the Acm2 interaction, we measured the forces between the enzyme and peptidoglycan purified from *B. subtilis*, which is structurally similar to that of *L. plantarum* (Fig. 3 *a*) (22,28). Topographic imaging showed that the morphology of peptidoglycan-coated surfaces was homogeneous and stable upon repeated scanning, indicating strong attachment of the macromolecules (Fig. 3 *b*). Imaging a small area at large force removed the peptidoglycan layer and made it possible to assess its thickness, which was ~1.3 nm (Fig. 3 *b*, *open square*). Force-distance curves recorded at a retraction speed of 1000 nm/s between Acm2 and *B. subtilis* peptidoglycans (Fig. 3 *c*) showed substantial binding (7%) in the form of single adhesion events with a magnitude of 56 ± 23 pN and a rupture length of ~50 nm. Hence, binding signatures were similar to those measured on *L. plantarum* cells (Fig. 2). Given the length of the spacer molecule (6 nm), the 50 nm rupture distances essentially reflect extension of the protein and/or peptidoglycan. In contrast, a truncated version of Acm2 lacking the SH3b domain (Acm2ΔSH3) showed very poor binding (1%), demonstrating that this domain is essential for the Acm2-peptidoglycan interaction (Fig. 3 *d*).

As specific binding forces between receptors and ligands depend on the loading rate, i.e., the rate at which the force is applied to the complex (27,29), we measured the Acm2 binding forces as a function of the loading rate. Fig. 3 *e* shows that the mean adhesion force (F) increased linearly with the logarithm of the loading rate (r), as observed for other receptor-ligand systems (27,29), including peptidoglycan-vancomycin (12) and peptidoglycan-LysM interactions (13). The length scale of the energy barrier, x_β, was assessed from the slope, f_β ($1.1 \pm 0.2 \times 10^{-11}$), of the F versus $\ln(r)$ plot and found to be 0.37 nm, i.e., in the range of values (0.2–1 nm) typically measured by single-molecule AFM (27). Extrapolation to zero forces yielded $r_{F=0}$ (8.9×10^{-12}) and, in turn, the kinetic off-rate constant of dissociation at zero force: $k_{\text{off}} = r_{F=0}\, x_\beta / k_B T = 0.8\ \text{s}^{-1}$. This fast off-rate suggests that Acm2 dissociates rapidly from its substrate and thus that the interaction is highly dynamic.

We also found that the binding frequency increased exponentially with contact time, to reach a constant-value plateau after only 0.5 s (Fig. 3 *f*), indicating that formation of the Acm2-peptidoglycan bond is fast. The time dependency may reflect the time necessary for conformational changes within both molecules to achieve optimal fitting. From this plot, we found the interaction time needed for half-maximal probability of binding, $t_{0.5}$, to be 0.17 s,

which in turn allowed us to estimate the association rate constant, $k_{on} = {t_{0.5}}^{-1} N_A V_{eff} = 1.6 \times 10^3\ M^{-1}\ s^{-1}$, where V_{eff} is the effective volume explored by the tip-tethered Acm2 (approximated here to a half-sphere of 6 nm radius, i.e., the spacer length). Considering the above rate constants, we then estimated the equilibrium dissociation constant to be $K_D = k_{off}/k_{on} = 0.5$ mM. This value should be considered with caution, considering the errors on the dynamic force spectroscopy data. However, it is several orders of magnitude larger than values obtained for other protein-ligand systems like antibody-antigen or drug-protein pairs (in the micromolar to nanomolar range), suggesting that Acm2 binds peptidoglycan with low affinity. The low binding affinity of Acm2 could enable the enzyme to rapidly detach and bind new peptidoglycan target sites, thus helping it to efficiently fulfill its enzymatic function.

Acm2 binds to structurally different peptidoglycans and to chitin

What is the substrate-binding specificity of Acm2? Does it bind to structurally different peptidoglycans? Does it recognize only the glycan chains, the peptide bridges, or both? To answer these questions, we measured the binding forces between Acm2 and peptidoglycans purified from *S. aureus* and *M. luteus*, both structurally different from the *B. subtilis* and *L. plantarum* peptidoglycans. As can be seen in Fig. 4, the binding properties (binding probability and binding strength) were in both cases very similar to those observed on the *B. subtilis* peptidoglycan. As repetition of the disaccharide GlcNAc-MurNAc is a common part in the three peptidoglycans, this finding suggests that Acm2 binds to this component, the peptide stem residues playing no major role in the interaction.

To confirm that the glycan backbone is the general structure bound by Acm2, we measured its interaction toward chitin, a polymer of GlcNAc reminiscent of the glycan chain of peptidoglycan (Fig. 5). Force-distance curves recorded at a retraction speed of 1000 nm/s between Acm2 and chitin (Fig. 5 *c*) showed a large fraction (21%) of single binding events with a magnitude of 64 ± 13 pN and rupture length of 50–150 nm, which were essentially abolished by addition of free GlcNAc monosaccharides (adhesion frequency drops from 21% to 2%) (Fig. 5 *d*). In addition, we observed a strong dependence of adhesion force and adhesion frequency on the loading rate and interaction time, respectively. The slope, f_β ($1.1 \pm 0.2 \times 10^{-11}$), and extrapolation to zero force, $r_{F=0}$ (9.2×10^{-12}) enabled us to extract values for the energy barrier, $x_\beta = 0.38$ nm, and the kinetic parameters $k_{off} = 0.8\ s^{-1}$, $k_{on} = 0.6 \times 10^3\ M^{-1}\ s^{-1}$, and $K_D = 1.5$ mM. These data suggest that Acm2 binds to chitin and the glycan backbone of peptidoglycan with affinities that are in the same range.

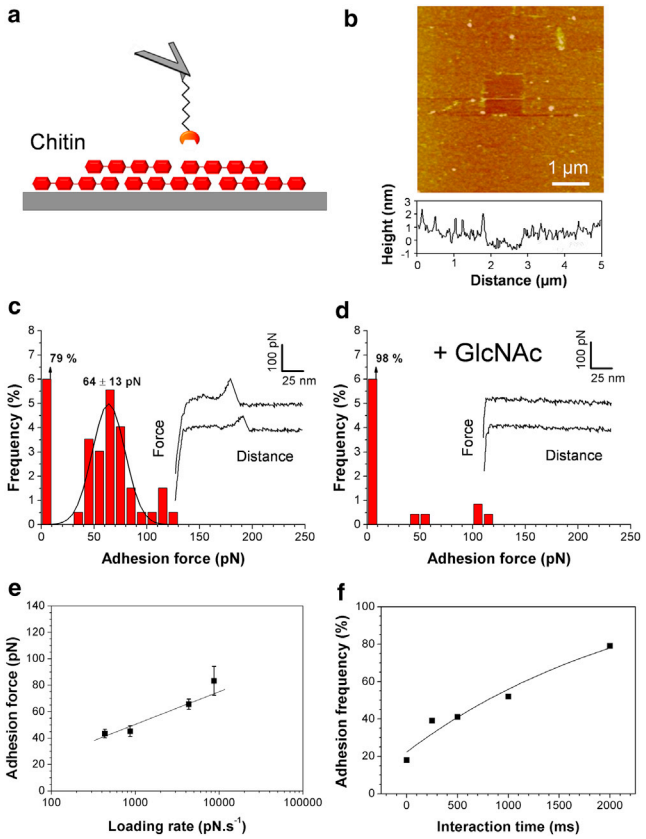

FIGURE 5 Strength and dynamics of the Acm2-chitin interaction. (*a*) Strategy for measuring the Acm2-chitin interaction. (*b*) AFM height image ($z = 15$ nm; a vertical cross section taken in the center of the image is shown beneath the image) recorded with a silicon nitride tip documenting the presence of smooth, ~1.6-nm-thick layer of chitin. (*c*) Adhesion-force histogram ($n = 200$) together with representative force curves, recorded in buffer between an Acm2 tip and a chitin surface. (*d*) Same experiment performed in the presence of 1 mM GlcNAc. (*e*) Dependence of the adhesion force on the loading rate applied during retraction (mean ± SE). (*f*) Dependence of the adhesion frequency on the interaction time, measured at a constant retraction speed of 1000 nm/s. Only the curves showing single-molecule adhesion events were considered. Similar plots were obtained in duplicate experiments using different tips and substrates.

Glucosamine is the minimal binding motif of Acm2

To determine the minimal binding motif recognized by Acm2, we performed a series of inhibition experiments using five monosaccharides of increasing structural complexity: glucose (Glc); glucosamine (GlcN); muramic acid (Mur), which is the ether between GlcN and lactic acid; and the *N*-acetyl derivatives of GlcN and Mur, GlcNAc and MurNAc. Fig. 6 shows that the adhesion frequency and mean adhesion force measured for the Acm2-peptidoglycan interaction were not altered by addition of Glc. By contrast, addition of GlcN, Mur, GlcNAc, or MurNAc always led to a dramatic reduction of adhesion frequency (from 92% to 99%), indicating that these sugars are equally bound by Acm2. Because GlcN is the common part in these four

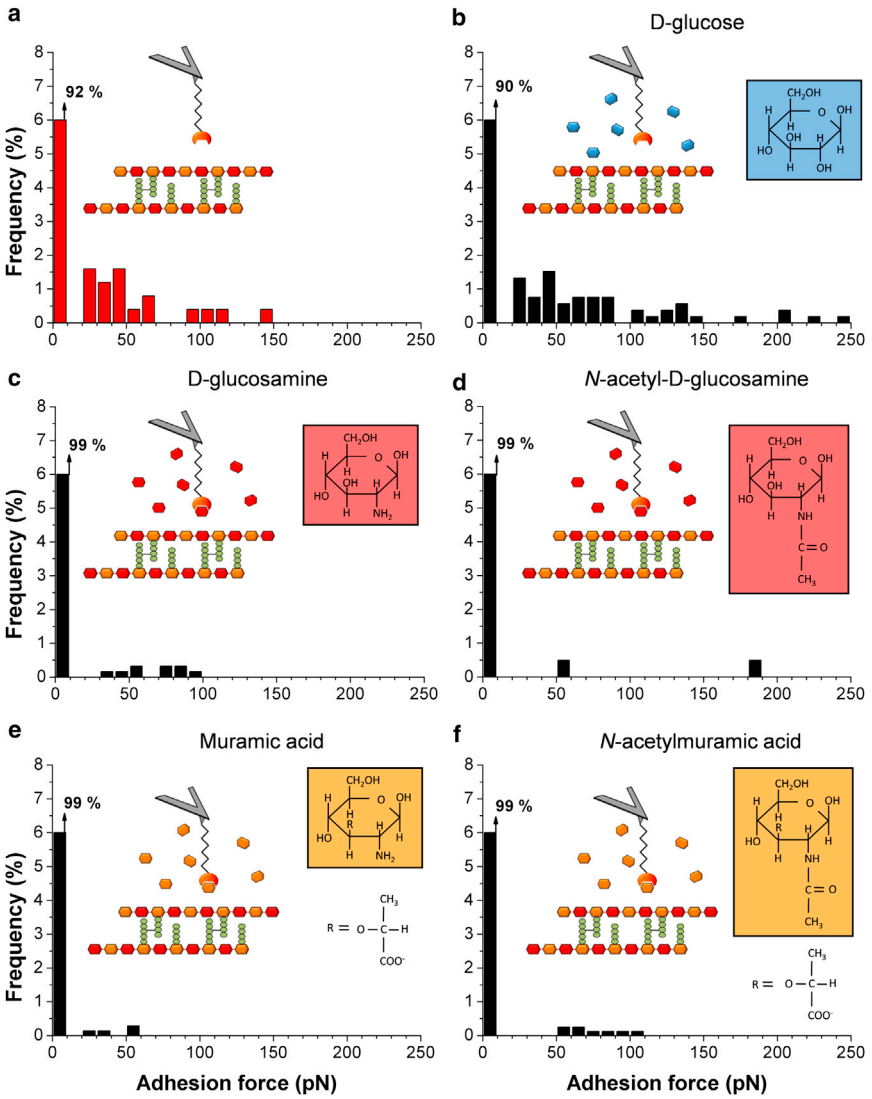

FIGURE 6 Inhibition experiments identify the minimal binding motif of Acm2. (*a*) Adhesion-force histogram ($n = 600$) between an Acm2 tip and a *B. subtilis* peptidoglycan surface recorded in buffer. (*b–f*) Same type of data ($n = 600$ in each graph) obtained after blocking with structurally related monosaccharides (1 mM) Glc (*b*), GlcN (*c*), GlcNAc (*d*), Mur (*e*), and MurNAc (*f*). For each experiment, the same results were obtained in at least two independent analyses.

sugars, and Glc had no effect on the interaction, we conclude that GlcN is the minimal binding motif of Acm2, and that the amino group on the glucose backbone is of key importance for recognition.

Acm2 exhibits mucin-binding capacity

As mucin macromolecules that decorate host intestinal cells are highly glycosylated and rich in GlcNAc and other amino sugars (30), we postulated that Acm2 may also bind to this glycopolymer. As can be seen in Fig. 7, force measurements between Acm2 and mucin showed substantial binding (12%), with a mean adhesion force of 43 ± 6 pN, which was abolished by addition of free GlcNAc. Varying the loading rate (slope $f_\beta = 1.2 \pm 0.3 \times 10^{-11}$; length scale of the energy barrier, $x_\beta = 0.34$ nm; and extrapolation to zero force, $r_{F=0}$ (3.1×10^{-11}) and interaction time enabled us to determine the affinity of the Acm2-mucin interaction ($k_{off} = 2.5\ s^{-1}$, $k_{on} = 3.0 \times 10^3\ M^{-1}\ s^{-1}$, and $K_D = 0.8$ mM), which was quite similar to that of the peptidoglycan interaction. Overall, the slopes and intercepts that we obtained for the Acm2-peptidoglycan, Acm2-chitin, and Acm2-mucin systems suggest that these interactions have dissociation rates that are in the same range. Whether the mucin-binding capacity measured here is of biological relevance (e.g., cell adhesion function) remains to be elucidated.

CONCLUSIONS

Despite the important role that peptidoglycan hydrolases play in cell wall remodeling, the molecular details of their interaction with peptidoglycan remain poorly understood. Also, because there is increasing evidence that cell-wall hydrolases can play multiple roles (4,31–33), studying their multifunctional nature is a topic of growing interest in

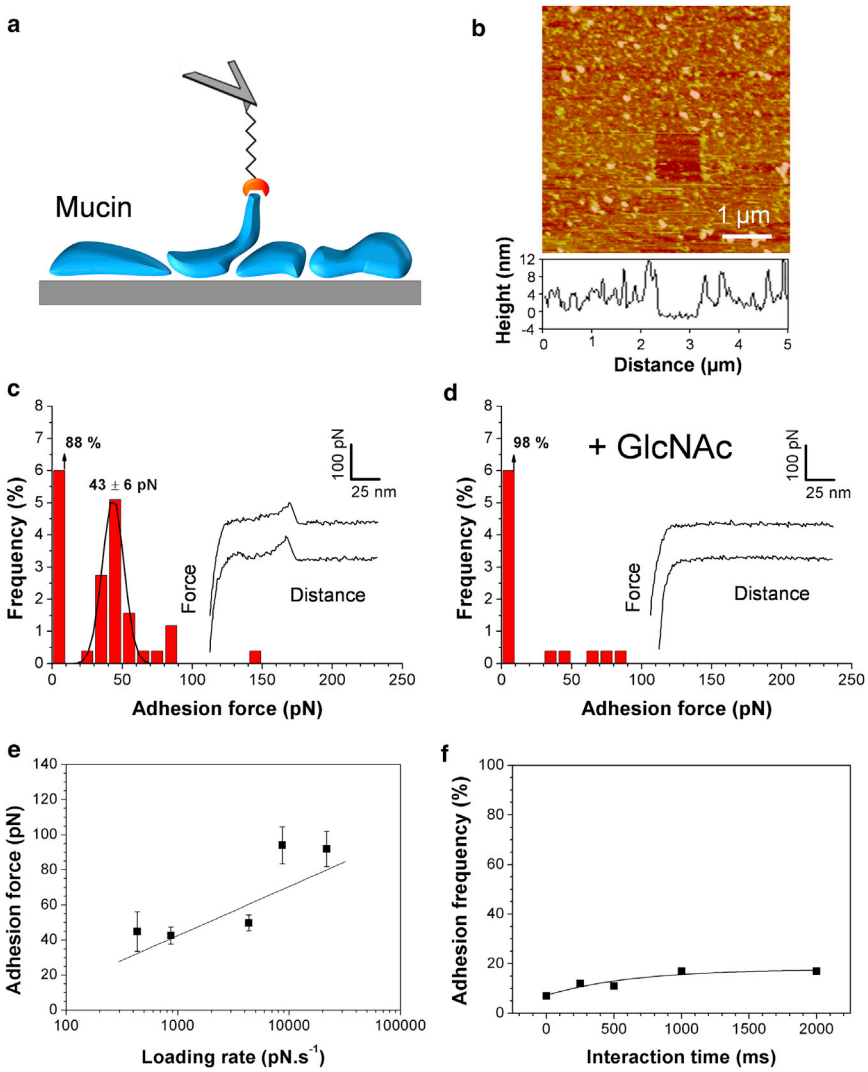

FIGURE 7 Acm2 exhibits mucin-binding properties. (*a*) Measuring the Acm2-mucin interaction. (*b*) AFM height image ($z = 30$ nm; a vertical cross section taken in the center of the image is shown beneath the image) recorded with a silicon nitride tip documenting the presence of an ~2.6-nm-thick layer of mucin. (*c*) Adhesion-force histogram ($n = 250$), with representative force curves, recorded in buffer between an Acm2 tip and a mucin surface. (*d*) Same experiment performed in the presence of 1 mM GlcNAc. (*e*) Dependence of the adhesion force on the loading rate applied during retraction (mean ± SE). (*f*) Dependence of the adhesion frequency on the interaction time, measured at a constant retraction speed of 1000 nm/s. Only the curves showing single-molecule adhesion events were considered. Similar plots were obtained in duplicate experiments using different tips and substrates.

current cell-wall research. Addressing these issues is an important step toward understanding the mechanisms by which peptidoglycan hydrolases control cell division and other cellular processes. To our knowledge, our single-molecule experiments provide novel insights into the binding mechanism of Acm2, and, more specifically, into the widely distributed (34), yet poorly understood, SH3b peptidoglycan-binding domain. Our main findings are as follows. 1), Consistent with its primary functional role, Acm2 causes major nanoscale alterations of the *L. plantarum* cell wall (increased roughness, septal erosion), leading eventually to cell lysis. 2), Acm2, most likely via its SH3b domain, specifically binds to bacteria and to purified peptidoglycan with low affinity (K_D in the mM range). 3), Glucosamine is the minimal binding motif, explaining why Acm2 binds to structurally different peptidoglycans and to chitin. 4), Acm2 also recognizes mucin, suggesting that in addition to its role in cell-wall remodeling, it may also display an adhesive function that could contribute to host colonization. As many eukaryotic proteins are decorated with amino sugars (35), we anticipate that Acm2 may bind to a broad range of glycoproteins.

We believe that the binding mechanism (low affinity, broad specificity) of Acm2 is of biological significance, as it may greatly contribute to a definition of Acm2 activity. On the one hand, like other peptidoglycan hydrolases, Acm2 has to fulfill two complementary actions, i.e., specific binding and hydrolysis of its substrate. Our finding that the enzyme binds its target with broad specificity and low affinity could be a widespread phenomenon among cell-wall hydrolases for regulating cell-wall remodeling during growth and division. On the other hand, bacterial cell-surface proteins mediate tight interactions between probiotics and their hosts (36). That Acm2 shows mucin-binding capacity therefore suggests that it is involved in bacterial-host interactions and is consistent with the fact that this enzyme is one of the most abundant cell-surface-associated proteins in *L. plantarum* (37).

The broad functionality of Acm2 suggested here would be consistent with the behavior of cell-wall hydrolases from several bacterial pathogens, including *S. epidermidis* AtlE and Aae (38), *S. saprophyticus* Aas (39), *S. aureus* Aaa (40,41), and *Listeria monocytogenes* Ami (42). In these enzymes, bacterial attachment is promoted by means of LysM and GW repeat domains. As the SH3b domain is widely distributed among probiotic and pathogenic species (34), we suggest that the binding characteristics highlighted here may represent a general mechanism among bacterial hydrolases for guiding cell division and cell adhesion.

We are grateful to Michiel Kleerebezem for providing the *cps1–4* mutant.

Work by the teams of Y.F.D. and P.H. was supported by the National Foundation for Scientific Research (FNRS), the Foundation for Training in Industrial and Agricultural Research (FRIA), the Université catholique de Louvain (Fonds Spéciaux de Recherche), the Federal Office for Scientific, Technical and Cultural Affairs (Interuniversity Poles of Attraction Programme), and the Research Department of the Communauté française de Belgique (Concerted Research Action). Y.F.D. and P.H. are Senior Research Associate and Research Associate of the FNRS.

REFERENCES

1. Vollmer, W., D. Blanot, and M. A. de Pedro. 2008. Peptidoglycan structure and architecture. *FEMS Microbiol. Rev.* 32:149–167.
2. Typas, A., M. Banzhaf, …, W. Vollmer. 2012. From the regulation of peptidoglycan synthesis to bacterial growth and morphology. *Nat. Rev. Microbiol.* 10:123–136.
3. Navarre, W. W., and O. Schneewind. 1999. Surface proteins of gram-positive bacteria and mechanisms of their targeting to the cell wall envelope. *Microbiol. Mol. Biol. Rev.* 63:174–229.
4. Vollmer, W., B. Joris, …, S. Foster. 2008. Bacterial peptidoglycan (murein) hydrolases. *FEMS Microbiol. Rev.* 32:259–286.
5. Fredriksen, L., G. Mathiesen, …, W. Egge-Jacobsen. 2012. The major autolysin Acm2 from *Lactobacillus plantarum* undergoes cytoplasmic *O*-glycosylation. *J. Bacteriol.* 194:325–333.
6. Lu, J. Z., T. Fujiwara, …, J. Sakon. 2006. Cell wall-targeting domain of glycylglycine endopeptidase distinguishes among peptidoglycan cross-bridges. *J. Biol. Chem.* 281:549–558.
7. Xu, Q., S. Sudek, …, I. A. Wilson. 2009. Structural basis of murein peptide specificity of a γ-D-glutamyl-l-diamino acid endopeptidase. *Structure.* 17:303–313.
8. Gründling, A., and O. Schneewind. 2006. Cross-linked peptidoglycan mediates lysostaphin binding to the cell wall envelope of *Staphylococcus aureus*. *J. Bacteriol.* 188:2463–2472.
9. Tripathi, P., V. Dupres, …, Y. F. Dufrêne. 2012. Deciphering the nanometer-scale organization and assembly of *Lactobacillus rhamnosus* GG pili using atomic force microscopy. *Langmuir.* 28:2211–2216.
10. Turner, R. D., E. C. Ratcliffe, …, S. J. Foster. 2010. Peptidoglycan architecture can specify division planes in *Staphylococcus aureus*. *Nat. Commun.* 1:26.
11. Hinterdorfer, P., M. F. Garcia-Parajo, and Y. F. Dufrêne. 2012. Single-molecule imaging of cell surfaces using near-field nanoscopy. *Acc. Chem. Res.* 45:327–336.
12. Gilbert, Y., M. Deghorain, …, Y. F. Dufrêne. 2007. Single-molecule force spectroscopy and imaging of the vancomycin/D-Ala-D-Ala interaction. *Nano Lett.* 7:796–801.
13. Andre, G., K. Leenhouts, …, Y. F. Dufrêne. 2008. Detection and localization of single LysM-peptidoglycan interactions. *J. Bacteriol.* 190:7079–7086.
14. Andre, G., S. Kulakauskas, …, Y. F. Dufrêne. 2010. Imaging the nanoscale organization of peptidoglycan in living *Lactococcus lactis* cells. *Nat. Commun.* 1:27.
15. Engel, A., and H. E. Gaub. 2008. Structure and mechanics of membrane proteins. *Annu. Rev. Biochem.* 77:127–148.
16. Puchner, E. M., and H. E. Gaub. 2009. Force and function: probing proteins with AFM-based force spectroscopy. *Curr. Opin. Struct. Biol.* 19:605–614.
17. Andre, G., M. Deghorain, …, Y. F. Dufrêne. 2011. Fluorescence and atomic force microscopy imaging of wall teichoic acids in *Lactobacillus plantarum*. *ACS Chem. Biol.* 6:366–376.
18. Bernard, E., T. Rolain, …, M. P. Chapot-Chartier. 2011. Characterization of *O*-acetylation of *N*-acetylglucosamine: a novel structural variation of bacterial peptidoglycan. *J. Biol. Chem.* 286:23950–23958.
19. Dufrêne, Y. F. 2008. Atomic force microscopy and chemical force microscopy of microbial cells. *Nat. Protoc.* 3:1132–1138.
20. Ebner, A., L. Wildling, …, H. J. Gruber. 2007. A new, simple method for linking of antibodies to atomic force microscopy tips. *Bioconjug. Chem.* 18:1176–1184.
21. Palumbo, E., M. Deghorain, …, P. Hols. 2006. D-alanyl ester depletion of teichoic acids in *Lactobacillus plantarum* results in a major modification of lipoteichoic acid composition and cell wall perforations at the septum mediated by the Acm2 autolysin. *J. Bacteriol.* 188:3709–3715.
22. Rolain, T., E. Bernard, …, P. Hols. 2012. Identification of key peptidoglycan hydrolases for morphogenesis, autolysis, and peptidoglycan composition of *Lactobacillus plantarum* WCFS1. *Microb. Cell Fact.* 11:137.
23. Remus, D. M., R. van Kranenburg, …, M. Kleerebezem. 2012. Impact of 4 *Lactobacillus plantarum* capsular polysaccharide clusters on surface glycan composition and host cell signaling. *Microb. Cell Fact.* 11:149.
24. Rolain, T., E. Bernard, …, P. Hols. 2013. *O*-glycosylation as a novel control mechansim of peptidoglycan hydrolase activity. *J. Biol. Chem.* In press.
25. Touhami, A., M. H. Jericho, and T. J. Beveridge. 2004. Atomic force microscopy of cell growth and division in *Staphylococcus aureus*. *J. Bacteriol.* 186:3286–3295.
26. Francius, G., O. Domenech, …, Y. F. Dufrêne. 2008. Direct observation of *Staphylococcus aureus* cell wall digestion by lysostaphin. *J. Bacteriol.* 190:7904–7909.
27. Hinterdorfer, P., and Y. F. Dufrêne. 2006. Detection and localization of single molecular recognition events using atomic force microscopy. *Nat. Methods.* 3:347–355.
28. Atrih, A., and S. J. Foster. 1999. The role of peptidoglycan structure and structural dynamics during endospore dormancy and germination. *Antonie van Leeuwenhoek.* 75:299–307.
29. Merkel, R., P. Nassoy, …, E. Evans. 1999. Energy landscapes of receptor-ligand bonds explored with dynamic force spectroscopy. *Nature.* 397:50–53.
30. Johansson, M. E. V., D. Ambort, …, G. C. Hansson. 2011. Composition and functional role of the mucus layers in the intestine. *Cell. Mol. Life Sci.* 68:3635–3641.
31. Wyckoff, T. J., J. A. Taylor, and N. R. Salama. 2012. Beyond growth: novel functions for bacterial cell wall hydrolases. *Trends Microbiol.* 20:540–547.
32. Vollmer, W. 2012. Bacterial growth does require peptidoglycan hydrolases. *Mol. Microbiol.* 86:1031–1035.
33. Uehara, T., and T. G. Bernhardt. 2011. More than just lysins: peptidoglycan hydrolases tailor the cell wall. *Curr. Opin. Microbiol.* 14:698–703.
34. Layec, S., B. Decaris, and N. Leblond-Bourget. 2008. Diversity of Firmicutes peptidoglycan hydrolases and specificities of those involved in daughter cell separation. *Res. Microbiol.* 159:507–515.
35. Stanley, P. 2011. Golgi glycosylation. *Cold Spring Harb. Perspect. Biol.* 3:1–13.

36. Kleerebezem, M., P. Hols, …, P. A. Bron. 2010. The extracellular biology of the *lactobacilli*. *FEMS Microbiol. Rev.* 34:199–230.

37. Beck, H. C., S. M. Madsen, …, A. M. Hansen. 2009. Proteomic analysis of cell surface-associated proteins from probiotic *Lactobacillus plantarum*. *FEMS Microbiol. Lett.* 297:61–66.

38. Heilmann, C., G. Thumm, …, G. Peters. 2003. Identification and characterization of a novel autolysin (Aae) with adhesive properties from *Staphylococcus epidermidis*. *Microbiology.* 149:2769–2778.

39. Hell, W., H. G. W. Meyer, and S. G. Gatermann. 1998. Cloning of aas, a gene encoding a *Staphylococcus saprophyticus* surface protein with adhesive and autolytic properties. *Mol. Microbiol.* 29:871–881.

40. Heilmann, C., J. Hartleib, …, G. Peters. 2005. The multifunctional *Staphylococcus aureus* autolysin aaa mediates adherence to immobilized fibrinogen and fibronectin. *Infect. Immun.* 73:4793–4802.

41. Hirschhausen, N., T. Schlesier, …, C. Heilmann. 2012. Characterization of the modular design of the autolysin/adhesin Aaa from *Staphylococcus aureus*. *PLoS ONE.* 7:e40353.

42. Milohanic, E., R. Jonquières, …, J. L. Gaillard. 2001. The autolysin Ami contributes to the adhesion of *Listeria monocytogenes* to eukaryotic cells via its cell wall anchor. *Mol. Microbiol.* 39:1212–1224.